

## Biogenic synthesis of zinc oxide nanoparticles using leaves extract of *Camellia sinensis* for photocatalytic and biological applications

R. Sattar<sup>a</sup>, M. A. Rasool<sup>a</sup>, R. Qadir<sup>b\*</sup>, A. B. Siddique<sup>b</sup>, M. I. Irfan<sup>b</sup>, I. Saba<sup>c</sup>  
M. T. Akhtar<sup>b</sup>, M. M. ur Rehman<sup>a</sup>, M. Mustaqeem<sup>b</sup>

<sup>a</sup>Department of Chemistry, University of Lahore, Sargodha Campus, Sargodha, 40100, Pakistan

<sup>b</sup>Institute of Chemistry, University of Sargodha, Sargodha, 40100, Pakistan

<sup>c</sup>Department of Chemistry, GC Women University Sialkot-51310, Pakistan

Nanoparticles have attracted considerable attention of researchers due to their diverse properties in the fields of catalysis, energy devices, wound healing and drug delivery systems. Synthesis of nanoparticles using plants and microbial extract is a green approach due to easy handling, rapidity and cost-effectiveness. This article reported a simple and green method of zinc oxide nanoparticles (ZnO-NPs) synthesis using *Camellia sinensis* leaves extract as reducing agent. State-of-the-art techniques were utilized for the characterization and measure the potential applications of ZnO-NPs. FTIR and SEM analysis were performed to confirm the nature of bonding and morphology of NPs. XRD analysis confirmed the hexagonal wurtzite structure and crystallite size (34 nm) of ZnO-NPs. EDX analysis was performed to check the purity of NPs. Energy band gap of valence band and conduction band was found 3.278 eV using UV/Visible spectrophotometry. Purified ZnO-NPs were utilized to determine the photocatalytic potential for degradation of hazardous dye (methylene blue) at  $\lambda_{\max}$  of 668 nm under irradiation of sunlight. The results indicated ~92% photodecomposition of dye after 110 min of sunlight irradiation. Moreover, ZnO-NPs also revealed the antibacterial potential, having better inhibition power against gram-negative bacterial strains.

(Received October 14, 2022; Accepted January 2, 2023)

**Keywords:** Green synthesis, Dye degradation, Antibacterial potential, Disc diffusion method

### 1. Introduction

Synthesis and evaluation of potential applications of nanoparticles (NPs) is an emerging field since last decade. NPs are recognized for their significant role in the fields of energy, medicines, catalysis etc. Among different classes of NPs, semiconductor NPs have gained a prime importance due to their uses in display devices, energy storage devices and drug delivery applications etc. Due to quantum confinement effects and the high surface area, semiconductor-type nanoparticles possess enormous optical and antibacterial properties as compared to the large sized particles [1, 2].

ZnO is a semiconductor material with wide bandgap, having optical transparency and fluorescence in visible and near ultraviolet span of spectrum. So the electronic transition is possible in the ZnO nanoparticles even at room temperature. The optical bandgap of ZnO nanofilm decreases at high annealing temperature. Due to these properties, ZnO nanoparticles are applicable in solar cells, photocatalyst, optoelectronic and photonic devices etc. Annealing temperature influences the surface morphology of ZnO film. Zinc oxide can be used as photocatalyst for degradation of dyes under sunlight exposure [3]. ZnO NPs are also applicable in manufacturing of batteries and super-capacitors. Highly flexible super-capacitance of 118.122 mFcm<sup>-2</sup>, was obtained using ZnO fabricated electrodes. Thus, ZnO can be used in energy storage devices like batteries and capacitors [4]. Moreover, due to visible light assisted photocatalysis in ZnO

---

\* Corresponding author: rsumra@gmail.com  
<https://doi.org/10.15251/JOBM.2023.151.1>

nanoparticles, these nanoparticles found applications to control plant pathogen minimize food borne diseases and meet increasing demand of world population [5-7].

Many researchers have reported various pathways to synthesize ZnO-NPs; these methods may influence the morphology and size of NPs. ZnO-NPs can be synthesized via sol-gel, co-precipitation, and hydrothermal processes. Recent research on ZnO-NPs has revealed their excellent photocatalytic, biological, and morphological properties. However, the toxic chemicals used in chemical synthetic approach for the production of NPs have detrimental effects on environment and have limited use in medical applications [8]. Green synthesis of nanomaterials has recently received enormous attention because it is an effective, fast, single-step method that uses eco-friendly solvents and produces less hazardous materials [9,10].

Among the diverse applications of NPs, photodecomposition of hazardous organic dyes is an interesting area to be explored. Organic dyes are used in the textile industries during pigmentation process. 15% organic dyes are wasted during third phenomenon and pose serious environmental hazard. Organic dyes present in the effluents of industries like pigment, textile etc. also pose serious health issues in living organisms of water bodies and ultimately to human beings. Various organic and inorganic NPs have been reported to show catalytic potential to decompose dyes in sunlight and exposure under UV radiations, but ZnO-NPs have shown remarkable results as photocatalyst [11]. It is a semiconductor material with high photochemical reactivity and non-toxic nature [12]. High catalytic and biological potential of ZnO-NPs is believed due to the low energy bandgap  $\sim 3.3$  eV, which results in high excitation binding energy and enhancement of the catalytic efficiency. ZnO is n-type semiconductor [13] and has gained many intensions in materials and medical science due to its unique properties such as biological (antimicrobial, antifungal, anticancer, and antiviral properties), UV absorption, as well as stable thermal and optical properties that pose no environmental risk [14].

ZnO-NPs can be synthesized in different crystal phases but the most stable one is hexagonal wurtzite structure [15]. Over the years, several methods for synthesizing ZnO-NPs including chemical reduction [16], thermal decomposition [17], photochemical reduction [18], electrochemical [19], hydrothermal [20], laser irradiation [21], pyrolysis [22], etc. have been applied, but limitations like toxicity of chemicals and harsh synthetic conditions are associated with these methods [23]. Therefore, green synthesis of NPs using economical, environment friendly raw materials and solvents is a beneficial way. Moreover, green synthesis is suitable technique because stable hexagonal wurtzite structure ZnO-NPs are formed via this approach [24]. In green synthetic scheme, phenolics present in the plant extracts reduce and stabilize the NPs [25]. In addition to robustness of method, the NPs formed have improved physical and optical properties [26]. It has also been observed that the ZnO-NPs synthesized via this route have improved photocatalytic ability for decomposition of hazardous dyes [27-29]. The activity of NPs synthesized by using different plant extracts have also been checked against bacteria, where NPs revealed themselves as antibacterial agent with significant potential [30,31].

In the current research work, ZnO-NPs have been synthesized using extract of *Camellia sinensis* (green tea) leaves. Green tea leaves are easily available and extensively used for their wide applications due to presence of antioxidants and weight loss properties. Synthesized NPs were characterized by state-of-the-art spectroscopic techniques. Pure ZnO-NPs were examined for catalytic potential for photodecomposition of methylene blue (MB dye). Antibacterial activity of NPs was evaluated against gram-positive and gram-negative strains following disc diffusion method.

## 2. Experimental details

### 2.1. Chemicals and Reagents

All the chemicals used were of analytical grade; Zinc nitrate ( $\text{Zn}(\text{NO}_3)_2 \cdot 6\text{H}_2\text{O}$ ), ethanol ( $\text{C}_2\text{H}_5\text{OH}$ ), and methylene blue ( $\text{C}_{16}\text{H}_{18}\text{ClN}_3\text{S}$ ) were purchased from Sigma Aldrich. *Camellia sinensis* leaves were collected from the local market of Sargodha. Pakistan.

## 2.2. Synthesis of ZnO-NPs

Firstly, *Camellia sinensis* leaves were washed by double distilled water and air dried to remove the sand and dust impurities. Then, dried leaves were crushed into fine powder and screened through 300  $\mu\text{m}$  sieves. To prepare extract, 20 g *Camellia sinensis* leaves powder was mixed with 200 mL of double-distilled water and heated at 100  $^{\circ}\text{C}$  for 20 minutes with magnetic stirring. The mixture was cooled to room temperature, filtered, and centrifuged at 1500 rpm for 10 minutes to remove dense material. 50 mL of this extract was added to 30 mL of 0.5 M  $\text{Zn}(\text{NO}_3)_2 \cdot 6\text{H}_2\text{O}$  precursor solution. ZnO-NPs are formed after boiling the mixture for 2 h at 50  $^{\circ}\text{C}$  with constant magnetic stirring. Finally, the purified ZnO-NPs are obtained after centrifugation, filtration and washing with distilled water and ethanol. These NPs are dried at 35  $^{\circ}\text{C}$  for 24 hours and stored in air tight bottle.

## 2.3. Characterization

The ZnO-NPs were characterized by different spectroscopic and analytical techniques such as Fourier transform infrared spectroscopy (FTIR), UV/Visible spectroscopy (UV/Vis.), Powder X-ray diffraction (XRD), Scanning electron microscopy (SEM) and Energy-dispersive X-ray analysis (EDX). FTIR study was carried out using Bruker Tensor 27 FTIR spectrometer in the range of 400–4000  $\text{cm}^{-1}$ . It was used for functional group detection and nature of bond determination in extract and for comparison of spectra before and after the synthesis of NPs. XRD was used to characterize the crystallinity of the NPs at a scanning rate of 60  $\text{min}^{-1}$  using GNR, explorer X-ray diffractometer operating at 40.0 KV and current of 30 mA with monochromatized  $\text{Cu K}\alpha$  ( $\lambda=1.54187$  nm) monochromatic filter in the range between 20 - 70 $^{\circ}$ . Surface morphology and size of NPs was evaluated by Mira3, TESCAN scanning electron microscope. Photodecomposition of MB dye was studied using UV/Visible spectrophotometer LABOMED, INC. model number UVD- 2950.

## 2.4. Biological activity

Antibacterial potential of ZnO-NPs against gram-positive and gram-negative bacteria using *Escherichia coli*, *Pseudomonas aureus*, *Staphylococcus aureus*, and *Pseudomonas aeruginosa* strains was evaluated by disc diffusion method [32]. Ciprofloxacin drug was used as a positive control. The zone of inhibition in mm was measured against each bacterial strain.

## 3. Results and Discussion

### 3.1. FTIR and UV/Visible analysis

Phenolic components of plant extract are generally involved in the reduction and stabilization of NPs in green synthesis. Disappearance or decrease in intensity of broad –OH peak denotes the involvement of phenols in reduction phenomenon. The comparative FTIR spectra along with the major functional group peaks of extract before and after the synthesis of NPs is shown in Fig. 1(a) and Table S1. The broad round peak at 3200-3500  $\text{cm}^{-1}$  due to the stretching vibrations of -OH groups was observed due to presence of phenolic compounds. Peaks appeared in the range of 1487 and 1600  $\text{cm}^{-1}$  corresponded to C=C stretching in the aromatic ring and C=O in polyphenols. Moreover, weak peaks obtained in the range of 1051 and 802  $\text{cm}^{-1}$  were due to vibrations of C-O, C-N, and C-H groups. The characteristic weak peak at 490  $\text{cm}^{-1}$  indicated the presence of hexagonal phase of synthesized NPs.

Purified ZnO-NPs were utilized for recording of absorption spectra as shown in Fig. 1(b). Appearance of characteristic peak in absorption spectra at 378 nm confirmed the synthesis of ZnO-NPs. Energy band gap ( $E_{\text{bg}}$ ) between conduction band and valence band was found to be 3.278 eV. At this  $E_{\text{bg}}$  value, electron-hole pairs are easily formed for conduction which showed importance of these NPs as photocatalyst.

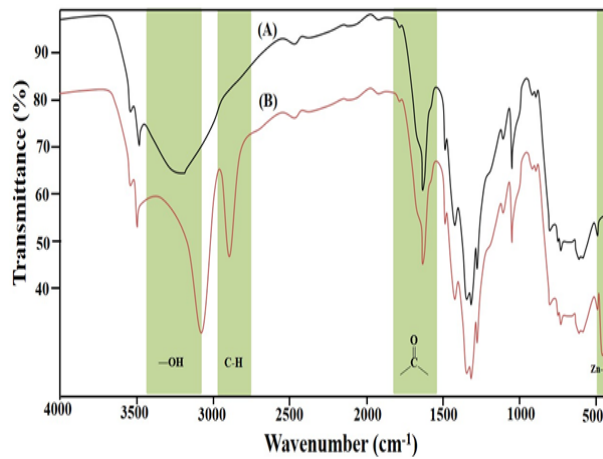


Fig. 1(a) (A) FTIR Spectrum of plant extract; (B) FTIR Spectrum of extract after ZnO-NPs synthesis.

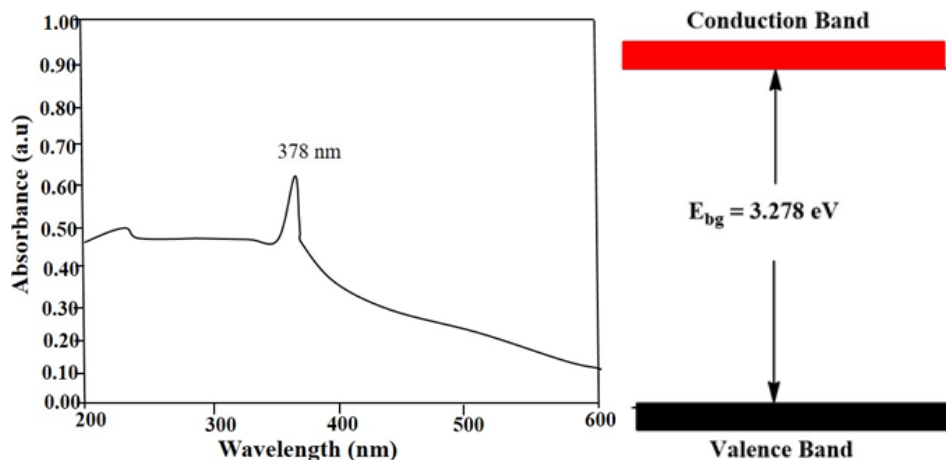


Fig. 1(b). UV/Visible Spectrum of ZnO-NPs

### 3.2. XRD analysis

The crystallinity of the NPs was investigated using XRD. XRD spectrum of biosynthesized ZnO-NPs is depicted in the Fig. 2. Three prominent diffraction peaks were observed at the  $2\theta$  value of  $32^\circ$  for (100) plane, at  $34.6^\circ$  for (002) plane, and at  $36.4^\circ$  for (101) plane attributed to the hexagonal wurtzite structure of ZnO-NPs. Other characteristics peaks observed at  $47.8^\circ$ ,  $56.9^\circ$ ,  $63^\circ$ ,  $66.5^\circ$ ,  $68.1^\circ$ , and  $69.2^\circ$  corresponds to (102), (110), (103), (200), (112), and (201), planes, respectively. Absence of any ambiguous peak in the pattern indicated the pure phase of ZnO-NPs. The sharp diffraction peaks confirmed the high crystallinity of NPs. The average crystallite size of NPs was found to be 34 nm, according to Scherrer's formula based on X-ray line broadening as shown in Eq (1),

$$D = \frac{0.9\lambda}{\beta \cos\theta} \quad (1)$$

where  $\lambda$  is measured in Å,  $\beta$  (full width at half maximum) in radian, and diffraction angle in degrees.

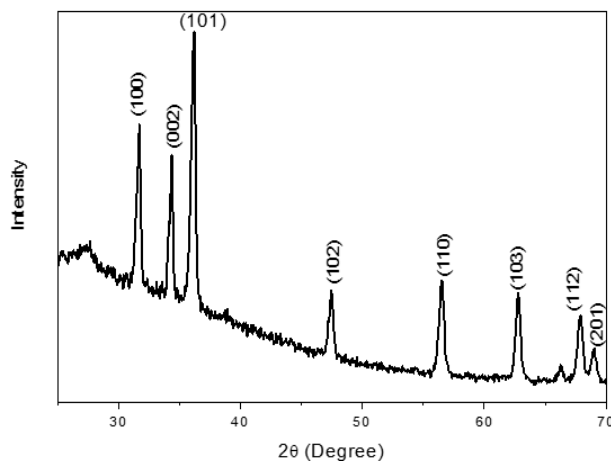


Fig. 2. XRD spectrum of ZnO-NPs.

### 3.3. SEM and EDX Analysis

SEM analysis was performed to examine the morphology of ZnO-NPs as shown in Fig. 3. The SEM results showed the spherical and elongated rod-type morphology of ZnO-NPs. The micrographs of NPs also revealed the morphology of different sizes of spherical nanoparticles and tendency of dense agglomeration. The EDX analysis confirmed the purity of ZnO-NPs by showing the only presence of zinc and oxygen elements in the sample. The % weight and atomicity of representative elements were depicted in Fig. 4.

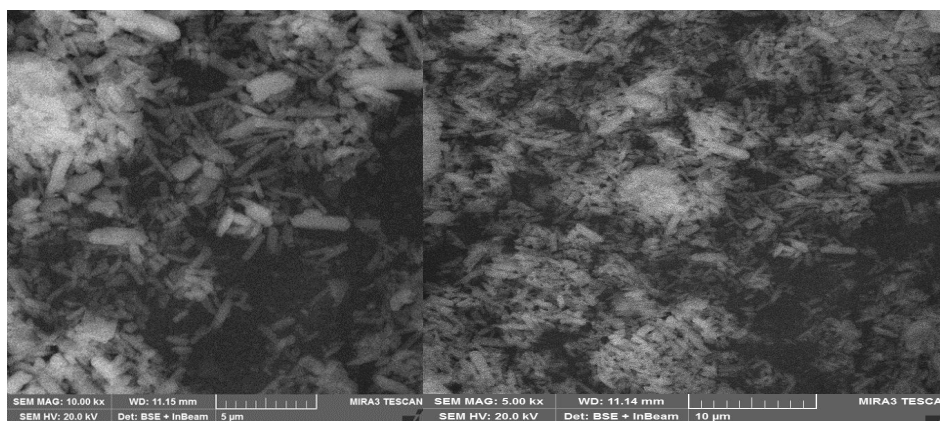


Fig. 3. SEM image of ZnO-NPs.

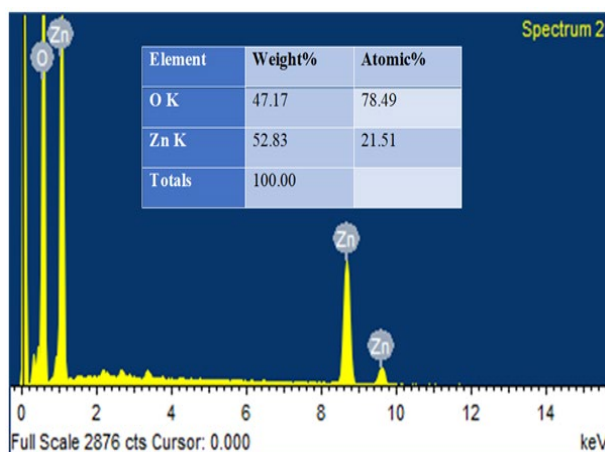


Fig. 4. EDX analysis of ZnO-NPs.

### 3.4. Photocatalytic Activity

ZnO-NPs are promising photocatalysts and can efficiently degrade hazardous dyes which are commonly used in textile industries. Photocatalytic potential of NPs was evaluated for photo-degradation of MB dye under sunlight. MB was taken as a probe molecule. 500 mg of catalyst (ZnO-NPs) was dispersed in 20 ppm aqueous solution of MB. Before irradiation to start adsorption-desorption equilibria, suspension of NPs was kept in the dark for 20-30 minutes. Then the suspensions were irradiated by sunlight in a reactor in a sequence of time intervals, for instance, at 0, 10, 20, 30, 40, 50, 70, 90 and 110 minutes, respectively and recorded for UV/Vis. spectrum. The variation in absorbance of light by MB dye in the presence of catalyst at different time intervals is shown in Fig. 5. Two broad peaks were present in the electronic spectra of MB and  $\lambda_{\text{max}}$  was monitored at 668 nm. Concentration of MB dye is decreased continuously with passage of time as depicted by absorbance values. It was hypothesized that catalytic potential of ZnO-NPs was due to more surface defects, high surface area and forming a space charge layer on the surface corresponded to photo-generated electrons and holes. The degradation efficiency was measured by using the following equation (2).

$$\text{Degradation (\%)} = C_o - \frac{C}{C_o} \times 100 = A_o - \frac{A}{A_o} \times 100 \quad (2)$$

where  $C_o$  symbolizes the initial concentration,  $C$  denotes the reaction concentration of dye,  $A_o$  denotes the initial absorbance, and  $A$  represents the changing absorbance of the dye at  $\lambda_{\text{max}}$ . After 110 minutes of photo irradiation, about 92% of organic dye (MB) was decomposed as represented in Fig. 6a.

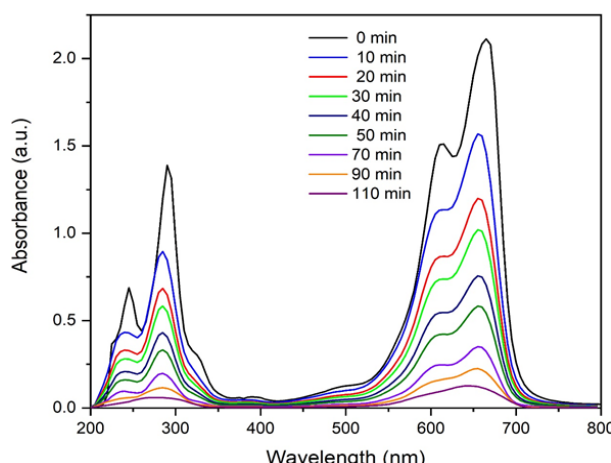


Fig. 5. Absorption spectra of MB dye for different irradiation time by ZnO-NPs.

For a better understanding of the photocatalytic degradation of MB, the reaction kinetics was studied. Photo-degradation reactions on catalytic surface generally follow pseudo-first-order kinetics, as shown by the equation (3).

$$\ln \frac{C_o}{C} = -kt \quad (3)$$

where  $C_o$ ,  $C$  and  $K$  represents the initial concentration ( $\text{mol L}^{-1}$ ) of the dye solution at 0 min, concentration ( $\text{mol L}^{-1}$ ) after different time intervals, the pseudo-first-order constant, respectively. The linear changes of  $\ln (C/C_o)$  w.r.t irradiation time in the degradation of MB confirmed the pseudo-first straight-line order kinetics (Fig. 6b). The MB dye degradation rate constant value ( $k$ ) was calculated as  $2.53 \times 10^{-2}$  per minute. These findings of photocatalytic study revealed the significant photocatalytic performance of the ZnO-NPs under sunlight. Therefore, these NPs can

be attributed as useful enduring photocatalyst for dye/organic pollutant removal from aqueous solution.

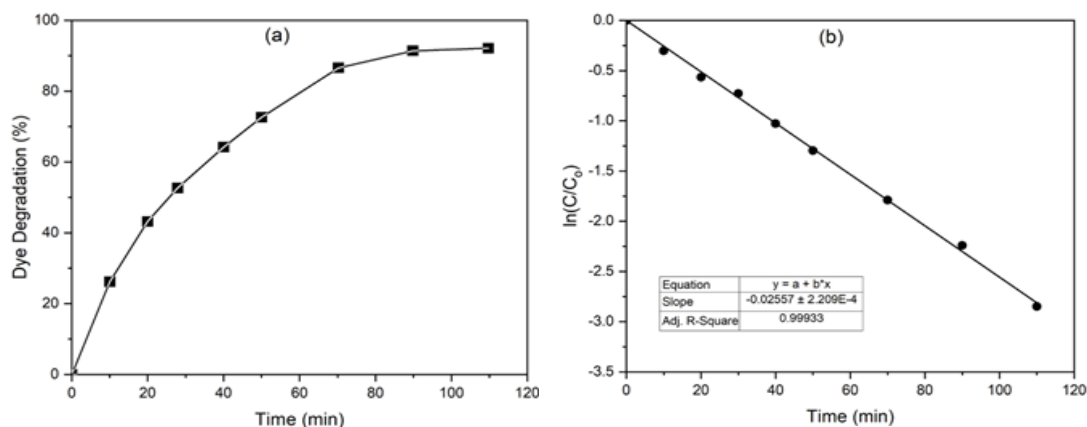


Fig. 6. (a) % photodegradation; (b) The reaction kinetics of MB dye for ZnO-NPs.

### 3.5. Antibacterial Activity

Antibacterial potential of the synthesized NPs was evaluated against gram-positive (*Staphylococcus aureus*, *Pseudomonas aeruginosa*) and gram-negative (*Escherichia coli*, *Pseudomonas aureus*) bacterial strains by following disc diffusion methods.

Bacteria-free filler discs were filled with 10  $\mu$ L of ZnO-NPs and were placed on the test strain inoculated agar at 37-38  $^{\circ}$ C for about 24 h. Ciprofloxacin drug was used as a positive control, while oil-free discs were used as a negative control. Zone of inhibition of each strain was measured which showed that the NPs inhibited the growth of gram-negative bacteria (*E. coli*) the most and gram-positive bacteria (*S. aureus*) the least. The antibacterial activity of NPs is due to the penetration of particles inside the bacterial cell by crossing the membrane barriers and inactivated of enzymes, producing hydrogen peroxide, which causes the death of bacterial cells. NPs were more active against gram-negative strains due to their thin cell wall. So, NPs could quickly penetrate and cause damage in these cells.

Table 1. Inhibition zones of bacterial growth.

	Zone of inhibition (mm)			
	Gram-Negative Bacteria		Gram-Positive Bacteria	
Sample	<i>E. coli</i>	<i>P. multocida</i>	<i>S. aureus</i>	<i>B. subtilis</i>
Plant Extract	10 $\pm$ 0.3	10 $\pm$ 0.4	9 $\pm$ 0.1	9 $\pm$ 0.1
ZnO-NPs	16 $\pm$ 0.2	14 $\pm$ 0.1	7 $\pm$ 0.3	8 $\pm$ 0.2
Ciprofloxacin (Standard)	28 $\pm$ 0.2	25 $\pm$ 0.01	21 $\pm$ 0.2	18 $\pm$ 0.3

## 4. Conclusion

The ZnO-NPs were successfully synthesized via biogenic method using *Camellia sinensis* leaves. The characteristic absorption peaks observed in UV/Vis. and FTIR spectrum indicated the formation of ZnO-NPs. The hexagonal wurtzite structure of ZnO-NPs was confirmed by XRD analysis. SEM and EDX analysis confirmed the purity, spherical and rod-type morphology of ZnO-NPs. The ZnO-NPs exhibited better photocatalytic performance ( $\sim$  92% degradation of MB dye after 110 minutes) under sunlight irradiation. Degradation kinetics studies suggested the photo-degradation of MB dye as pseudo-first order reaction with rate constant value ( $k$ ) = 2.53

$\times 10^{-2} \text{ min}^{-1}$ . The significant photocatalytic performance of ZnO-NPs makes them appealing candidate for organic dye removal from textile industry waste. The synthesized ZnO-NPs also exhibited potent antibacterial activities particularly against gram-negative bacterial strains.

## References

- [1] T.K. Pathak, R.E. Kroon, H.C. Swart, *Vacuum*, 157, 508 (2018); <https://doi.org/10.1016/j.vacuum.2018.09.020>
- [2] T.K. Pathak, E. Coetsee-Hugo, H.C. Swart, C.W. Swart et al., *Mater Sci Eng B*, 261, 114780 (2020); <https://doi.org/10.1016/j.mseb.2020.114780>
- [3] R. Biju, R. Ravikumar, C. Thomas, C.R. Indulal, *J Nanopart Res*, 24, 1 (2022); <https://doi.org/10.1007/s11051-022-05495-3>
- [4] J. Yan, G. Wang, H. Wang, Z. Zhang et al., *J Nanopart Res*, 17, 1 (2015); <https://doi.org/10.1007/s11051-015-2870-3>
- [5] C.B. Ong, L.Y. Ng, A.W. Mohammad, *Renew Sust Energ Rev*, 81, 536 (2018); <https://doi.org/10.1016/j.rser.2017.08.020>
- [6] M.T. Islam, A. Dominguez, B. Alvarado-Tenorio et al., *ACS omega*, 4, 6560 (2019); <https://doi.org/10.1021/acsomega.9b00023>
- [7] P. Mitra, D. Dutta, S. Das, T. Basu et al., *ACS omega*, 3, 7962 (2018); <https://doi.org/10.1021/acsomega.8b00568>
- [8] N.M. Ngoepe, Z. Mbita, M. Mathip et al., *Ceramics International*, 44, 16999 (2018); <https://doi.org/10.1016/j.ceramint.2018.06.142>
- [9] F. Davar, A. Majedi, A. Mirzaei, *J Am Ceram Soc*, 98, 1739 (2015); <https://doi.org/10.1111/jace.13467>
- [10] M. Shabaani, S. Rahaiee, M. Zare, S.M. Jafari, *Lwt-Food Sci Technol*, 134, 110133 (2020); <https://doi.org/10.1016/j.lwt.2020.110133>
- [11] J.J. Feng, Z.Z. Wang, Y.F. Li et al., *J Nanopart Res*, 15, 1(2013); <https://doi.org/10.1007/s11051-013-1565-x>
- [12] C.A. Soto-Robles, P.A. Luque, C.M. Gómez-Gutiérrez et al., *Results Phys*, 15, 102807 (2019); <https://doi.org/10.1016/j.rinp.2019.102807>
- [13] M.S. Khan, P.P. Dhavan, D. Ratna, N.G. Shimpi, *J Clust Sci*, 33, 1007 (2022); <https://doi.org/10.1007/s10876-021-02036-1>
- [14] A.C. Dhanmozhi, V. Rajeswari, S. Sathyajothi, *Proc*, 4, 660 (2017); <https://doi.org/10.1016/j.matpr.2017.01.070>
- [15] A. Manohar, J. Park, D.D. Geleta et al., *J Alloys Compd*, 874, 159868 (2021); <https://doi.org/10.1016/j.jallcom.2021.159868>
- [16] I. Hussain, N.B. Singh, A. Singh et al., *Biotechnol Lett*, 38, 545 (2016); <https://doi.org/10.1007/s10529-015-2026-7>
- [17] L.R. Yadav, B. Archana, K. Lingaraju et al., *Int J Nanosci*, 15, 1650013 (2016); <https://doi.org/10.1142/S0219581X16500137>
- [18] M. Nilavukkarasi, S. Vijayakumar, S. Prathipkumar, *Mater Sci Energ Technol*, 3, 335 (2020); <https://doi.org/10.1016/j.mset.2019.12.004>
- [19] M. Manokari, M.S. Shekhawat, *World Sci. News*, 69, 111 (2017).
- [20] N. Srivastava, M. Srivastava, P.K. Mishra, P.W. Ramteke, *Front Microbiol*, 7, 514 (2016); <https://doi.org/10.3389/fmicb.2016.00514>
- [21] S.A. Ealia, M.P. Saravanakumar, *Mater Sci Eng C*, 263, 032019 (2017); <https://doi.org/10.1088/1757-899X/263/3/032019>
- [22] H. Agarwal, S.V. Kumar, S. Rajeshkumar, *Resour-Effic Technol*, 3, 406 (2017); <https://doi.org/10.1016/j.reffit.2017.03.002>
- [23] M. Zare, K. Namratha, M.S. Thakur, K. Byrappa, *Mater Res Bull*, 109, 49 (2019);

<https://doi.org/10.1016/j.materresbull.2018.09.025>

[24] S.A. Khan, F. Noreen, S. Kanwal et al., Mater Sci Eng C, 82, 46 (2018);

<https://doi.org/10.1016/j.msec.2017.08.071>

[25] N.H. Nguyen, V.V. Padil, V.I. Slaveykova et al., Nanoscale Res Lett, 13, 1 (2018);

<https://doi.org/10.1186/s11671-017-2411-3>

[26] S. Ahmed, S.A. Chaudhry, S. Ikram, J Photochem Photobiol B Biol, 166, 272 (2017);

<https://doi.org/10.1016/j.jphotobiol.2016.12.011>

[27] A.U. Khan, Q. Yuan, Y. Wei et al., J Photochem Photobiol B Biol, 159, 49 (2016);

<https://doi.org/10.1016/j.jphotobiol.2016.03.017>

[28] Z. U. Khan, A. Khan, A. Shah, Y. Chen et al., J Photochem Photobiol B Biol, 156, 100

(2016); <https://doi.org/10.1016/j.jphotobiol.2016.01.016>

[29] T. Bhuyan, K. Mishra, M. Khanuja et al., Mater Sci Semicond Process, 32, 55 (2015);

<https://doi.org/10.1016/j.mssp.2014.12.053>

[30] J. Santhoshkumar, S.V. Kumar, S. Rajeshkumar, Resource-Efficient Technologies, 3, 459

(2017); <https://doi.org/10.1016/j.reffit.2017.05.001>

[31] K. Tahir, S. Nazir, B. Li et al., J Photochem Photobiol B Biol, 164, 164 (2016);

<https://doi.org/10.1016/j.jphotobiol.2016.09.030>

[32] A. Kourmouli, M. Valenti, E. van Rijn, H.J. Beaumont et al., J Nanopart Res, 20, 1 (2018);

<https://doi.org/10.1007/s11051-018-4152-3>